JVSTB Journal of Vacuum Science & Technology B

Gain saturation and carrier distribution effects in molecular beam epitaxy grown Ga As Sb ⁄ Ga As quantum well lasers

S.-Q. Yu, X. Jin, S. R. Johnson, and Y.-H. Zhang

Citation: Journal of Vacuum Science & Technology B **24**, 1617 (2006); doi: 10.1116/1.2192534
View online: http://dx.doi.org/10.1116/1.2192534
View Table of Contents: http://scitation.aip.org/content/avs/journal/jvstb/24/3?ver=pdfcov
Published by the AVS: Science & Technology of Materials, Interfaces, and Processing

Gain saturation and carrier distribution effects in molecular beam epitaxy grown GaAsSb/GaAs quantum well lasers

S.-Q. Yu, X. Jin, S. R. Johnson,[a] and Y.-H. Zhang
Center for Solid State Electronics Research and Department of Electrical Engineering, Arizona State University, Tempe, Arizona 85287-6206, Tempe, Arizona 85287-6206

(Received 14 September 2005; accepted 5 December 2005; published 31 May 2006)

GaAsSb/GaAs quantum well (QW) lasers grown by solid source molecular beam epitaxy are fabricated into ridge lasers and tested. These devices have a lasing wavelength around 1.2 μm that is substantially blueshifted relative to the electroluminescence peak. The magnitude of the blueshift increases as the cavity length is shortened, indicating that the blueshift increases with injection level. This blueshift is attributed to material gain saturation and band filling effects. The internal quantum efficiency is ~75%, the transparency current density is ~120 A/cm^2, and the threshold characteristic temperature is ~60 K, all typical for GaAsSb/GaAs based edge emitting lasers. The extracted gain constant is ~800 cm^{-1} for single QW active regions and approximately half that amount for double QWs. This discrepancy is attributed to nonuniform carrier distribution in double QW structures. © *2006 American Vacuum Society.* [DOI: 10.1116/1.2192534]

I. INTRODUCTION

Vertical-cavity surface-emitting lasers (VCSELs) operating at 1.3 μm are of great interest for low-cost data transmission applications such as fiber to home, local area networks, and free-space optical interconnects. GaAs is the preferred substrate for 1.3 μm VCSELs because it is compatible with the growth of near lattice-matched GaAs/AlGaAs distributed Bragg reflectors (DBRs) which have superior optical and thermal properties compared to other III-V DBRs. Furthermore, the fabrication of GaAs based 1.3 μm VCSELs can take full advantage of the current industry standard 850 nm VCSEL fabrication technology, which is attractive from a manufacturing point of view. GaAsSb/GaAs quantum wells (QWs) have been shown to be one of the most suitable candidates for 1.3 μm active regions on the GaAs substrate.[1–11]

To further improve VCSEL performance, it is necessary to understand the limitations of this material system and the interaction of the various parameters that impact overall device performance. For example, the gain of this material system is restricted by a less than ideal electron-hole wave function overlap caused by a combination of strongly confined holes and weakly confined electrons, which is a result of a nearly flat conduction band alignment between GaAs and GaAsSb.[12] When multiple QWs are used to increase modal gain, this strong hole confinement can influence the uniformity of the carrier distribution in each well. Furthermore, GaAsSb/GaAs QWs are highly strained (~2.7%) at the composition necessary for 1.3 μm emission. This not only limits the maximum QW number that can be grown without misfit dislocations, but also results in strain-driven in-plane composition fluctuations, which can reduce quantum efficiency and increase inhomogeneous linewidth broadening. The quality of highly strained GaAsSb layers can be improved by adding GaAsP strain compensation layers[2,13–15] near the active region. To date the best performing GaAsSb/GaAs based edge-emitting lasers (EELs) and VCSELs have been demonstrated[10,11] using GaAsP strain compensating layers.

In this article, three typical EELs grown by molecular beam epitaxy (MBE) are studied; one with a single GaAsSb/GaAs QW, one with a strain compensated single GaAsSb/GaAs/GaAsP QW, and one with two strain compensated GaAsSb/GaAs/GaAsP QWs. The internal quantum efficiency, the internal loss, the transparency current density, the material gain constant, and the characteristic temperatures of the threshold current density and the slope efficiency are measured and compared for these three devices.

II. EXPERIMENTAL RESULTS

The EELs studied in this work were grown on (100) n^+ GaAs substrates using solid source MBE. Device A has an active region containing one GaAs/$GaAs_{0.7}Sb_{0.3}$/GaAs (5 nm/7 nm/5 nm) QW grown at 490 °C, device B has an active region containing one $GaAs_{0.9}P_{0.1}$/GaAs/$GaAs_{0.7}Sb_{0.3}$/GaAs/$GaAs_{0.9}P_{0.1}$ (8 nm/3 nm/7 nm/3 nm/8 nm) QW grown at 500 °C, and device C has an active region containing two QWs of the same structure as device B also grown at 500 °C. The nominal Sb concentration is 30%, a value estimated from photoluminescence (PL) measurements and modeling. The active region in device A is sandwiched between two 30 nm $Al_{0.25}Ga_{0.75}As$ layers, followed by two 150 nm thick AlGaAs layers with a linearly graded Al mole fraction from 25% to 65% to form a graded-index (GRIN) waveguide, followed by Si-doped (2×10^{18} cm^{-3}), 1.8 μm thick, n-type $Al_{0.65}Ga_{0.35}As$ cladding and 500 nm thick GaAs buffer layers on the substrate side and Be-doped (2×10^{18} cm^{-3}), 1.8 μm thick, p-type $Al_{0.65}Ga_{0.35}As$ cladding and 100 nm thick GaAs contact layers on the top side. The doping concentration is decreased from 2×10^{18} to 1×10^{17} in both the p and n GRIN layers and is increased to

[a]Author to whom correspondence should be addressed; electronic mail: shane.johnson@asu.edu

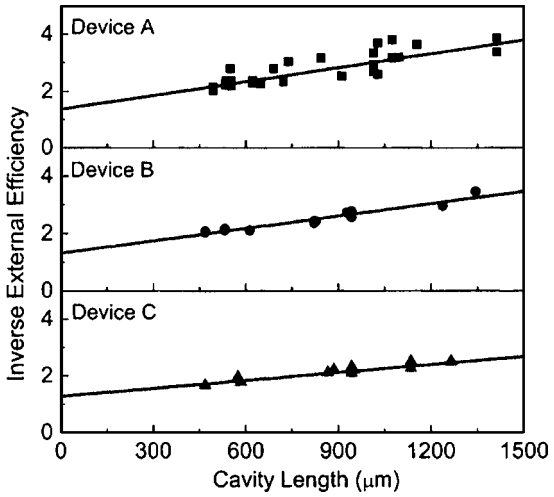

FIG. 1. Inverse external quantum efficiency vs cavity length for a single QW laser without strain compensation (solid squares), a single QW laser with strain compensation (solid circles), and a double QW laser with strain compensation (solid triangles). The solid line is a linear fit to the data, where internal quantum efficiency and internal loss are fitting parameters.

2×10^{19} in the p contact layer. Devices B and C have the same structure and doping profile as device A, except that the QW in device B (device C) is sandwiched between two 78 nm (65 nm) thick $Al_{0.25}Ga_{0.75}As$ layers. The active region growth temperatures were optimized to give the strong PL and minimal inhomogeneous linewidth broadening. Further details of the growth of this material system can be found in previous work.[10–12,14,15]

The devices were fabricated using photolithography and inductance coupled plasma (ICP) dry etching to define stripe ridges, ranging from 4 to 32 μm wide. By etching down through the p-GaAs contact layer and stopping about 0.1 μm above the active region, these ridges provide current confinement as well as waveguiding. A photoresist mask is used to define the ridges, which also serves as a lift-off mask for the deposition of an Al_2O_3 isolation layer. This procedure ensures that a self-aligned contact window is exposed after lift-off. Next wide Ti/Pt/Au p-contact stripes are deposited using a second mask, after which the wafers are lapped down to 100 μm and AuGe/Ni/Au n-metal contacts are deposited on the backside of the substrate; this is followed by rapid thermal annealing for both metal contacts. The wafers were cleaved to form EEL devices with various cavity lengths. The as-cleaved devices were mounted junction-side up on a metal test stage and are driven by a pulsed current source using a 0.5 μs wide pulse and a 0.1% duty cycle. The power output was measured using a calibrated power meter equipped with an InGaAs detector and an integration sphere.

Light power output versus current (L-I) measurements were done on 32 μm wide devices with different cavity lengths. The inverse external quantum efficiency $1/\eta_e$ versus the cavity length L is plotted in Fig. 1. The internal quantum efficiency η_i and the internal loss α_i are extracted by fitting the following relation to the data (fit given by the solid curve):

TABLE I. Internal quantum efficiency η_i internal loss α_i, transparency current density J_{tr}, and gain constant G_0.

	Device A	Device B	Device C
η_i (%)	73	76	78
α_i (cm^{-1})	13	12	8
J_{tr} (A/cm^2)	127	119	131
G_0 (cm^{-1})	787	801	421

$$\frac{1}{\eta_e}=\frac{1}{\eta_i}\left[1+\frac{\alpha_i\cdot L}{\ln(1/\sqrt{R_1R_2})}\right], \tag{1}$$

where R_1 and R_2 are the mirror reflectivity, both equal to 0.33 for uncoated mirrors. All device cavity lengths are longer than 450 μm to minimize errors caused by gain saturation. The extracted internal quantum efficiency and loss for devices A, B, and C are 73% and 13 cm^{-1}, 76% and 12 cm^{-1}, and 78% and 8 cm^{-1}, respectively. A summary of the extracted device characteristic is given in Table I. A substantial amount of the internal loss ($\sim$6 cm^{-1}) is attributed to free carrier absorption in the relatively heavily doped cladding layer. The variation in the remaining portion of the internal loss is attributed to processing variations. The internal quantum efficiency of these devices is higher than previous reported values[5,6,9,13] for the same material system. We believe this is due to improved material quality through optimization of material growth and to slightly lower Sb concentrations.

The device temperature characteristics are determined from temperature dependent pulsed L-I measurements over a 0–90 °C range using a thermoelectric temperature stage. The threshold current density characteristic temperature T_0 and external quantum efficiency characteristic temperature T_1 were extracted by plotting the threshold current density and the external quantum efficiency versus temperature, respectively. The extracted T_0 and T_1 for long cavity devices are listed in Table II. All three devices give similar values around 60 K for T_0, which is in agreement with most published work for GaAsSb QWs.[5,6,9,13,16,17] Considering the improved internal efficiency of these devices, we believe that this value for T_0 reflects the intrinsic temperature property of this material system.

The material gain was evaluated by plotting threshold current density J_{th} versus the total loss α_{tot} in Fig. 2. The material gain constant G_0 and the transparency current density J_{tr} for devices A, B, and C are extracted by fitting the following equation to the data (see solid curve):

TABLE II. Cavity length L, lasing threshold characteristic temperature T_0, and slope efficiency characteristic temperature T_1

	Device A	Device B	Device C
L (μm)	1563	1344	1265
T_0 (K)	59	66	66
T_1 (K)	70	110	82

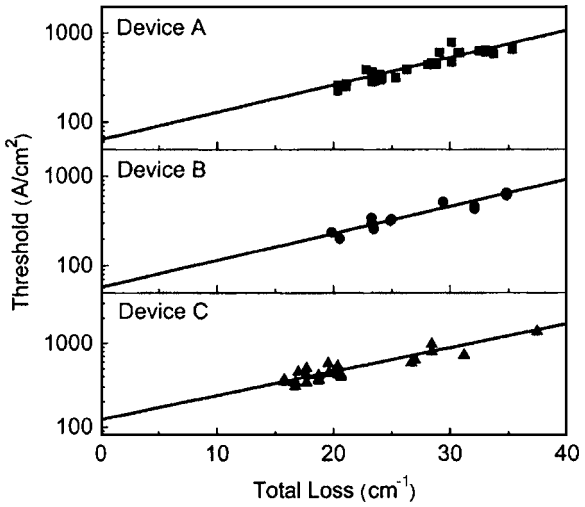

FIG. 2. Current density vs total loss for a single QW laser without strain compensation (solid squares), a single QW laser with strain compensation (solid circles), and a double QW laser with strain compensation (solid triangles). The solid line is an exponential fit to the data, where the gain constant and the transparency current density are fitting parameters.

$$J_{\text{th}} = \left(\frac{n_W J_{\text{tr}}}{\eta_i}\right) \exp\left[\frac{1}{(n_W \Gamma_W G_0)} \alpha_{\text{tot}} - 1\right]. \tag{2}$$

Here n_W is QW number and Γ_W is the optical confinement factor for each QW, which is determined to be 0.018 for all three devices using the slab waveguide theory. The extracted gain constant and transparency current density are 787 cm^{-1} and 127 A/cm^2, 801 cm^{-1} and 119 A/cm^2, and 421 cm^{-1} and 131 A/cm^2 for devices A, B, and C, respectively, which are lower than the previously reported values.[5] These results are in agreement except for the gain constant of the double QW laser (device C) which is surprisingly low, since, for example, devices B and C have similar structures (other than number of QWs) and were grown and fabricated back to back using the same process. The number of QWs appears in two places in Eq. (2); once with J_{tr} and once with G_0. Assuming that device C behaves like an $n_W=2$ laser in terms of loss and an $n_W=1$ laser in terms of gain, the fit results return a gain constant and transparency density of 842 cm^{-1} and 131 A/cm^2, which agree with the single QW lasers. These results indicate that the carriers are not uniformly distributed in the double QW active region. Since the GaAsSb/GaAs heterojunction has a very large valence band offset, this nonuniformity is most likely a result of inadequate hole transport.

The electroluminescence (EL) and lasing spectra of devices A, B, and C were measured for different cavity lengths at low injection and just above threshold, respectively, starting with the longest cavity. The same device is then cleaved into several shorter cavity length devices and then measured. This preparation process excludes any possible wavelength variations due to wafer nonuniformity. The devices are driven by a pulsed current source using a 0.5 μs wide pulse and a 1% duty cycle. The signal is collected using a 200 μm core diameter multimode fiber and is analyzed with an Ando 6315A optical spectrum analyzer using a 1 nm resolution setting. The measured spectra for various device lengths are shown in Fig. 3; device A in plot (a), device B in plot (b), and device C in plot (c). There is a blueshift in the lasing wavelength relative to the EL peak position that increases as the threshold current density increases for the shorter cavity

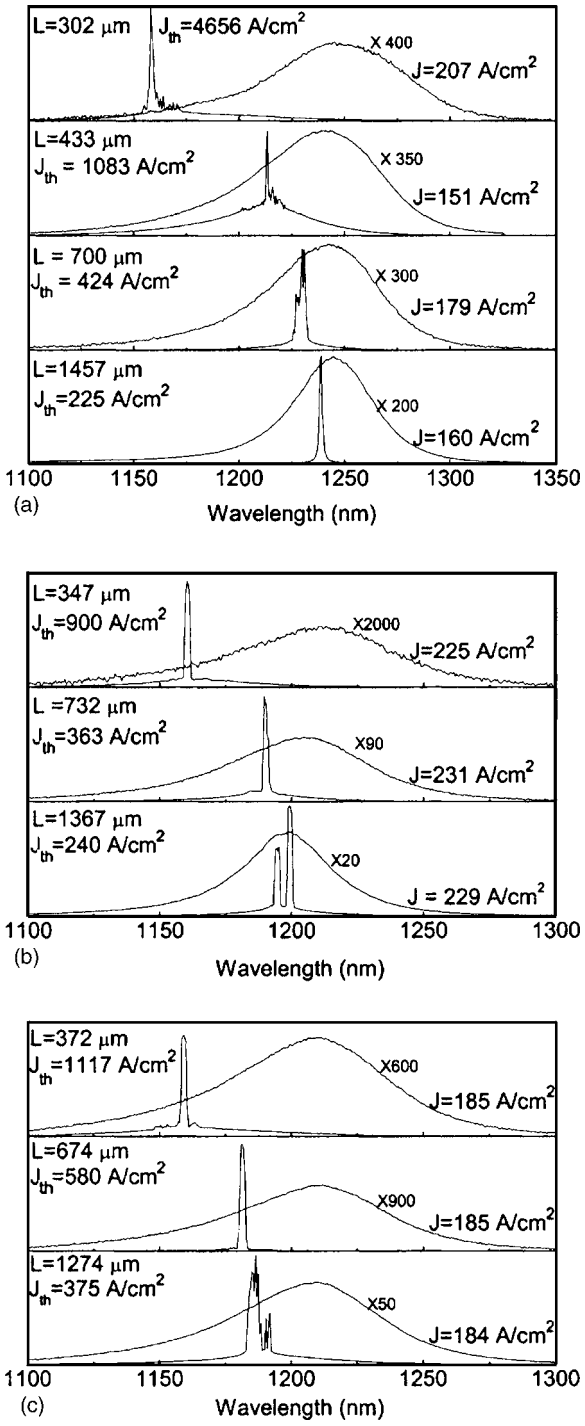

FIG. 3. Electroluminescence spectra under low injection and lasing spectra at threshold for different cavity length devices, showing a blueshift in lasing wavelength that increases with injection level. Plot (a) is for a single QW laser without strain compensation (device A), plot (b) is for a single QW laser with strain compensation (device B), and plot (c) is for a double QW laser with strain compensation (device C).

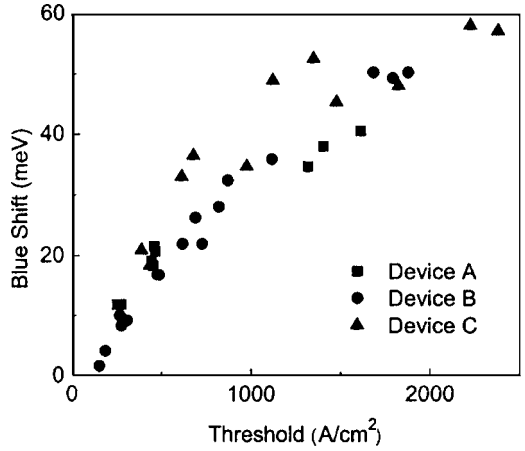

FIG. 4. Threshold lasing blueshift vs threshold current density for a single QW laser without strain compensation (solid squares), a single QW laser with strain compensation (solid circles), and a double QW laser with strain compensation (solid triangles).

devices, indicating gain saturation, which is typical for lower gain materials.[18] The EL peaks exhibit a small redshift as the laser cavity gets shorter; this is attributed to a drop in active region carrier density caused by an increase in leakage current density in the shorter devices.

The lasing wavelength blueshift versus the lasing threshold current density for the different cavity length devices is summarized in Fig. 4. The origin of the blueshift is likely due to gain saturation and band filling, which are exacerbated by a high density of localized tail states caused by in-plane composition fluctuations in the GaAsSb QWs. The low injection luminescence linewidth for all three devices is about 55 meV, and is in the middle to low range of the typical 40–80 meV values observed, which vary depending on the extent of strain-driven Sb segregation.[14] Here Sb segregation was minimized by using strain compensation in devices B and C and by growing the active region 10 °C lower in device A. The growth of these highly strained QWs is a trade off between excess inhomogeneous linewidth broadening and diminished internal quantum efficiency, where segregation can be reduced using lower growth temperatures, with the penalty of increased material defects. The double QW device unexpectedly shows a similar sized blueshift trend to that of the single QW devices. Under the same injection current density, the injection per QW, and consequently any band filling related blueshift, is expected to be smaller in a double QW device. Again these results point to only one QW contributing to lasing in the double QW device, likely due to a nonuniform carrier density in the active region.

III. DISCUSSION

The examination of gain saturation and gain blueshift under high injection is important for VCSEL design, since modal gain and gain spectrum/cavity mode matching are paramount in VCSEL performance. In the use of GaAsSb/GaAs active materials for VCSEL applications, two important observations are presented in this work: (i) the lasing wavelength blueshift with injection level and (ii) the lack of improvement in modal gain with the addition of a second QW. The injection dependent blueshift indicates band filling and gain saturation, both of which are aggravated by limited material gain and material inhomogeneities that are evident from the low injection linewidth. The lack of improvement in modal gain when a second QW is added is evident from both the gain constant and the blueshift measurements, which points to a nonuniform carrier distribution that results in one of the two QWs achieving gain while the other is at best transparent. In the worst case, the additional QW provides loss, which has been reported in three QW GaN based blue lasers.[19] Our results do not provide information on how carriers are distributed, though insufficient hole transport seems to be the most likely reason.

The phenomena of material gain saturation in GaAsSb/GaAs QWs and nonuniform carrier distribution in double QWs present a dilemma for VCSEL active region design: since single QWs do not provide sufficient modal gain, a straightforward solution is to incorporate more QWs to increase modal gain; however, increasing the QW number does not necessarily increase the modal gain when the carrier distribution is not uniform. In VCSELs there are intrinsic processes that can reduce carrier distribution nonuniformity, such as reabsorption of stimulated emission and active region heating. In the case of reabsorption, an absorbing QW will become transparent through optical pumping from the high optical field in the VCSEL cavity. In the case of active region heating, the probability of thermionic emission of holes from one QW to the other increases with temperature.

IV. CONCLUSIONS

The performance characteristics for three edge-emitting laser structures with a single GaAsSb/GaAs QW, a single strain compensated GaAsSb/GaAs/GaAsP QW, and a double strain compensated GaAsSb/GaAs/GaAsP QW active region are compared. These devices laser at around 1.2 μm and exhibit internal quantum efficiencies of up to 78%, the highest value reported to date for this material system. The threshold current density characteristic temperature is determined to be around 60 K and is thought to reflect the intrinsic temperature property of this material system, since the internal quantum efficiency is sufficiently high that defect related Shockley-Read-Hall recombination is not dominant. Two key observations are ascertained from gain constant and lasing blueshift measurements regarding the use of GaAsSb/GaAs active materials for laser applications: (i) there is a substantial blueshift in the gain peak with injection level, resulting from band filling and gain saturation, and (ii) there is a lack of improvement in modal gain with the addition of a second QW, resulting from inadequate carrier injection into one of the two QWs.

[1]T. Anan, K. Nishi, S. Sugou, M. Yamada, K. Tokutome, and A. Gomyo, Electron. Lett. **34**, 2127 (1998).
[2]P. Dowd *et al.*, Appl. Phys. Lett. **75**, 1267 (1999).
[3]T. Anan, M. Yamada, K. Tokutome, S. Sugou, K. Nishi, and A. Kamei,

Electron. Lett. **35**, 903 (1999).
[4]T. Anan, M. Yamada, K. Nishi, K. Kurihara, K. Tokutome, A. Kamei, and S. Sugou, Electron. Lett. **37**, 566 (2001).
[5]O. Blum and J. F. Klem, IEEE Photonics Technol. Lett. **12**, 771 (2000).
[6]S. Ryu and P. D. Dapkus, Electron. Lett. **36**, 1387 (2000).
[7]F. Quochi, D. C. Kilper, J. E. Cunningham, M. Dinu, and J. Shah, IEEE Photonics Technol. Lett. **13**, 921 (2001).
[8]Z. B. Chen *et al.*, Conference on Lasers and Electro-Optics Technical Digest, 2001, Vol. 1, p. 209.
[9]P.-W. Liu, M.-H. Lee, H.-H. Lin, and J.-R. Chen, Electron. Lett. **38**, 1354 (2002).
[10]P. Dowd *et al.*, Electron. Lett. **39**, 987 (2003).
[11]S.-Q. Yu *et al.*, Conference on Lasers and Electro-Optics Technical Digest, 2004, Vol. 1, p. 2.
[12]J.-B. Wang *et al.*, Phys. Rev. B **70**, 195339 (2004).
[13]M. S. Noh, R. D. Dupuis, D. P. Bour, G. Walter, and N. Holonyak, Appl. Phys. Lett. **83**, 2531 (2003).
[14]S. R. Johnson *et al.*, J. Vac. Sci. Technol. B **19**, 1501 (2001).
[15]X. H. Zheng, D. S. Jiang, S. R. Johnson, and Y.-H. Zhang, Appl. Phys. Lett. **83**, 4149 (2003).
[16]M. Yamada, T. Anan, K. Tokutome, A. Kamei, K. Nishi, and S. Sugou, IEEE Photonics Technol. Lett. **12**, 774 (2000).
[17]S. Ryu and P. D. Dapkus, Electron. Lett. **38**, 564 (2002).
[18]G. Park, O. Shchekin, and D. G. Deppe, IEEE J. Quantum Electron. **36**, 1065 (2000).
[19]K. Domen, R. Soejima, A. Kuramata, K. Horino, S. Kubota, and T. Tanahashi, Appl. Phys. Lett. **73**, 2775 (1998).